This is a repository copy of *Soft Ultraviolet (UV) Photopatterning and Metallization of Self-Assembled Monolayers (SAMs) Formed from the Lipoic Acid Ester of α-Hydroxy-1-acetylpyrene: The Generality of Acid-Catalyzed Removal of Thiol-on-Gold SAMs using Soft UV Light.*.

White Rose Research Online URL for this paper:
http://eprints.whiterose.ac.uk/116216/

Version: Accepted Version

**Article:**

## Soft UV Photo-patterning and Metallization of Self-Assembled Monolayers Formed from the Lipoic Acid Ester of α-Hydroxy-1-acetylpyrene: The Generality of Acid Catalyzed Removal of Thiol-on-Gold SAMs using Soft UV Light.

**SCHOLARONE**™
Manuscripts

# Soft UV Photo-patterning and Metallization of Self-Assembled Monolayers Formed from the Lipoic Acid Ester of α-Hydroxy-1-acetylpyrene: The Generality of Acid Catalyzed Removal of Thiol-on-Gold SAMs using Soft UV Light

Laurynas Pukenas,[†] Panida Prompinit,[†,‡] Boda Nishitha,[§] Daniel J. Tate,[∥] N. D. Pradeep Singh,[§] Christoph Wälti,[⊥] Stephen D. Evans[†] and Richard J. Bushby[∥,*]

[†] Molecular and Nanoscale Physics, School of Physics and Astronomy, University of Leeds, Leeds, LS2 9JT, UK

[‡] National Nanotechnology Center (NANOTEC), National Science and Technology Development Agency, Klong Luang, Pathumthani 12120, Thailand

[§] Department of Chemistry, Indian Institute of Technology Kharagpur, Kharagpur 721302, West Bengal, India

[∥] School of Chemistry, University of Leeds, Leeds, LS2 9JT, UK

[⊥] Institute of Microwaves and Photonics, School of Electronic and Electrical Engineering, University of Leeds, Leeds, LS2 9JT, UK

**ABSTRACT:** Under a layer of 0.1M HCl in isopropanol, soft UV (365 nm) photolysis of the thiol-on-gold self-assembled monolayer (SAM) derived from the lipoic acid ester of α-hydroxy-1-acetylpyrene results in the expected removal of the acetylpyrene protecting group. By photolyzing through a mask this can be used to produce a patterned surface and, at a controlled electrochemical potential, it is then possible to selectively and reversibly electrodeposit copper on the photolyzed regions. Rather surprisingly, under these photolysis conditions, there is not only the expected photodeprotection of the ester but also partial removal of the lipoic acid layer which has been formed. In further studies, it is shown that this type of acid catalyzed photo-removal of SAM layers by soft UV is a rather general phenomenon and results in the partial removal of the thiol-on-gold SAM layers derived from other ω-thiolated carboxylic acids. However, this phenomenon is chain-length dependent. Under conditions in which there is a ~60% reduction in the thickness of the SAM derived from dithiobutyric acid, the SAM derived from mercaptoundecanoic acid is almost unaffected. The process by which the shorter chain SAM layers are partially removed is not fully understood since these compounds do not absorb significantly in the 365nm region of the spectrum! Significantly, this study shows that acid catalysis photolysis of thiol-on-gold SAMs needs to be used with caution.

**KEYWORDS**: *self-assembled monolayers, soft UV photolithography, 1-acetylpyrene, lipoic acid, photochemical deprotection, electrochemical metallization.*

## INTRODUCTION

Soft UV (~365 nm) photolysis of Self-Assembled Monolayers (SAMs) can be used to induce specific functional group transformations and to create well-defined patterns on both gold and silica substrates.[1-19] Surfaces can be patterned with two, three or four different functional groups,[11,16-18] made so that they have a gradient of chemical or physical properties[16] or patterned so that they are suitable for the spatially selective attachment of biomolecules or the spatially selective deposition of polymers, nanoparticles or metals. Compared to deep UV photopatterning of SAMs, or the production of patterned SAMs through microcontact printing, one of the advantages of using soft UV photopatterning is that, by exploiting double quantum processes, it is possible to create SAMs that are patterned on the nanometer scale; on a scale less than that of the wavelength of the light.[1,2,19] Another advantage of soft UV photochemistry comes in terms of drug delivery using up-converting nanoparticles. Biological tissue is relatively transparent to light at ~800 nm and, since up-converting nanoparticles can convert ~880 nm to ~365 nm light, this can be used to trigger release of drugs from SAM layers bound to the particles through soft-uv photocleavable linkers. The 800 nm light penetrates 'deep' within the biological tissues triggering selective photochemical release of the drugs at the point at which they are required.[3,4]

Although most workers have concentrated on the photochemistry of *ortho*-nitrobenzyl derivatives, almost any preparative photochemical reaction can be adapted for use in the SAM environment.[5,6] However, preparative photochemical reactions that give high yields in dilute solution do not necessarily give equally good yields in SAMs and the *ortho*-nitrobenzyl systems are a case in point. Unless the photo-cleavage is acid-catalyzed,[7,8] the yields for photolysis of *ortho*-nitrobenzyl SAMs are poor to moderate (50-80%). As a result workers have started to explore alternative photochemistries including the photoreduction of azides,[9] the photoreaction of azides with amines,[10] CH bond insertion reactions of benzophenone derivatives,[11,12] 2 + 2 and 4+4 photocycloaddition reactions[13,14] and the photocleavage reactions of N-alkyl picolinium (NAP) esters.[15] In this paper we explore yet another chemistry; the photocleavage of α-esters of 1-acetylpyrene.[20] Several mechanisms have been proposed for this and related acyl ester photocleavage reactions.[20,21] The simplest mechanism invokes heterolysis of the α-

carbon-to-oxygen bond as shown in Scheme 1.[20] A possible alternative mechanism is described in reference 21. Here, we show that the photolysis of SAMs of an $\alpha$-ester of 1-acetylpyrene can be used to create patterned surfaces and that it is then possible to selectively electrodeposit copper on the photolyzed regions. Our objective in investigating this system was to find a soft UV photolyzed patterned SAM that was easier to selectively metallize than the *ortho*-nitrobenzyl-based SAMs that we have studied previously.[2] This was based on the assumption that the photo-removal of a larger, bulkier 'protecting group' from the surface would produce a bigger contrast between the photolyzed and unphotolyzed regions. Metallization of patterned surfaces has attracted interest mainly from the standpoint of creating electrodes, contacts and interconnects for electronic devices, but this requires electroless deposition of the metal on non-conductive substrates.[22] Electrochemical deposition of metals on (necessarily) conductive substrates is mainly of interest from the standpoint of the creation of surfaces with controlled topology with interesting optical/plasmonic properties (e.g. for surface-enhanced Raman spectroscopy) and, potentially, also for the creation of substrates that can be used as 'masters' in nano-inprint lithography and in the control of wetability and of liquid crystal alignment.

## EXPERIMENTAL SECTION

**Materials.** Dichloromethane 99.9% (DCM), hydrogen peroxide (27.5 wt.%), ($\pm$)-$\alpha$-lipoid acid 99%, 1 M hydrochloric acid, isopropyl alcohol (IPA) 99.9% and copper (II) sulfate pentahydrate ($CuSO_4 \cdot 5H_2O$) 99.995% were used as received from Sigma-Aldrich. Sulfuric acid (98%) was supplied by Fisher Scientific. Glass microscope slides (thickness 0.8 mm) were purchased from Agar and were cut to approximately three-quarters of the original length. Millipore Milli-Q water with a resistivity better than 18.1 M$\Omega$·cm was used throughout. High purity (99.99%) temper-annealed gold wire (0.75 mm diameter) was supplied by Goodfellow. Column chromatography employed Merck Geduran Si 60 as the stationary phase.

**Synthesis** (Scheme 1). A solution of 1-(bromoacetyl)pyrene (500 mg, 1.6 mmol), potassium carbonate (513 mg, 3.7 mmol) and racemic lipoic acid (514 mg, 3.1 mmol) in anhydrous acetone (25 mL) was

stirred at room temperature under an atmosphere of argon for 4 h. The reaction mixture was diluted with

EtOAc (100 mL) and the solution washed with saturated sodium hydrogen carbonate (2 × 30 mL), dried

(MgSO$_4$) and concentrated *in vacuo* without heat. The NMR spectrum of this crude product showed that

it contained unreacted lipoic acid but no 1-(bromoacetyl)pyrene. It was purified by rapid passage

through a very short silica column  eluting with dichloromethane to afford the title compound as yellow

crystals (584 mg, 84%). Recrystallization from EtOH/CHCl$_3$ gave bright yellow needles: mp 100-101

°C; IR (ATR,) 3048, 2929, 1739, 1686, 1594, 1583 cm$^{-1}$. $^1$H NMR (500 MHz, CDCl$_3$) $\delta$ 8.95 (d, $J$ = 9.4

Hz, 1H), 8.30 – 8.23 (m, 4H), 8.19 -8.15 (m, 2H), 8.09 - 8.05 (m, 2H), 5.47 (s, 2H, C$^2$$H_2$), 3.50 (quint., $J$

= 6.8 Hz, 1H, C$^{3''}$$H$), 3.19 - 3.12 & 3.11 – 3.04 (2 × m, 2 × 1H, C$^{5''}$$H_2$), 2.53 (t, $J$ = 7.3 Hz, 2H, C$^{2'}$$H_2$),

2.40 & 1.87 (approx. 2 x dq, $J$ = 12.4, ~ 6.6 Hz, 2 × 1H, C$^{4''}$$H_2$), 1.76 – 1.69  (m, 2H, C$^{3'}$$H_2$), 1.69 -1.62

(m, 2H, C$^{5'}$$H_2$), 1.55 – 1.39 (m, 2H, C$^{4'}$$H_2$); $^{13}$C NMR (75 MHz, CDCl3) $\delta$ 196.5 (ketone carbonyl),

173.1 (ester carbonyl), 134.3, 131.0, 130.5, 130.1, 130.0, 129.9, 128.5, 127.0, 126.6, 125.7, 125.0,

124.5, 124.1, 123.9, 67.8 (C$^2$), 56.2 (C$^{3''}$), 40.1 (C$^{4''}$), 38.4 (C$^{5''}$), 34.5 (C$^{2'}$), 33.7 (C$^{5'}$), 28.6 (C$^{4'}$), 24.6

(C$^{3'}$) (assignments based on2-D NMR studies). HRMS (EI, 70 eV) calcd. for C$_{26}$H$_{24}$O$_3$S$_2$ [M] 448.1167,

found 448.1149 (100%); [M+1] 449.1187 (20%). Anal. calcd for C$_{26}$H$_{24}$S$_2$O$_3$: C, 69.61; H, 5.39; S,

14.30%. Found: C, 69.30; H, 5.30; S, 14.15%.
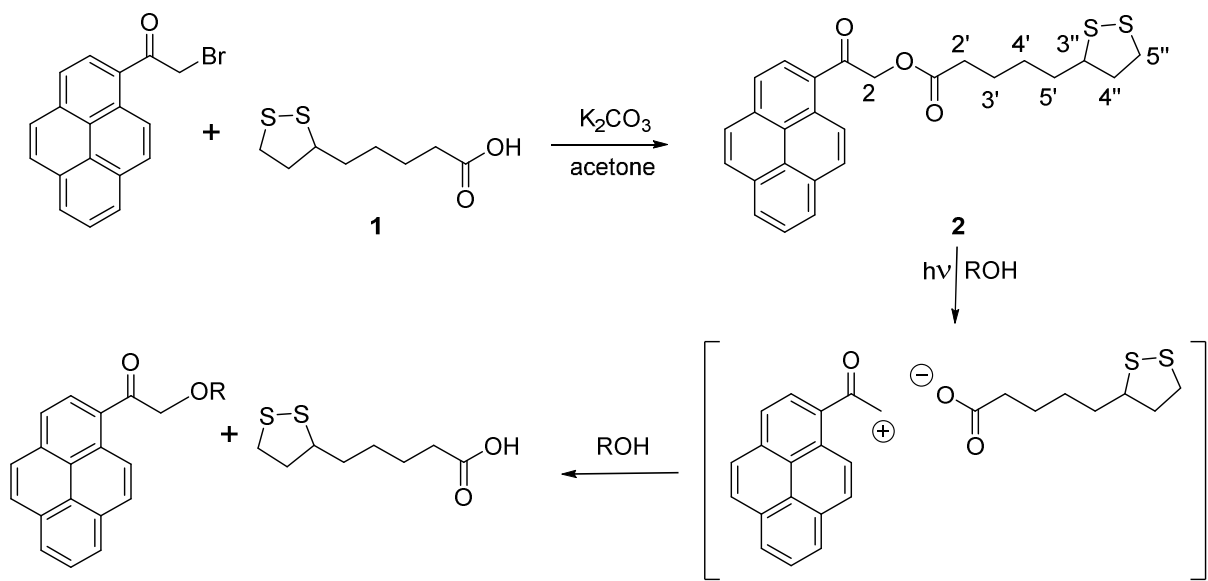
**Scheme 1.** Synthesis of pyrene ester **2**, the numbering system followed for the spectroscopic assignments, the photocleavage in alcohol solvents and the ion pair intermediate which is probably involved in the reaction mechanism.[16]

**Cyclic voltammetry**. Cyclic voltammetry was used to compare the reduction potentials of the ester **2** and of nitrobenzene using a dichloromethane solution, scanning at 100 mV s$^{-1}$, on a BASI Epsilon electrochemical workstation with a three-electrode cell, Ag/AgNO$_3$ as reference electrode, platinum wire as counter electrode and glassy carbon working electrode, in nitrogen-purged, 0.1 M solution of tetrabutylammonium hexafluorophosphate as a supporting electrolye at room temperature.

**Substrate Preparation.** Glass microscope slides were first cleaned by ultrasonication for 15 min in a 10% solution of Decon90 in Milli-Q water. Each slide was rinsed 10 times in Milli-Q water and then dried under a stream of oxygen free nitrogen. The samples were ultrasonicated in dichloromethane for 15 min, removed and dried in a stream of zero grade nitrogen, rinsed under Milli-Q water, and immersed in piranha solution (70:30, v/v, H$_2$SO$_4$: H$_2$O$_2$) for 10 min. The substrates were then rinsed in Milli-Q water, dried under nitrogen, and placed in an Edwards Auto 306 thermal evaporator. A 150 nm gold layer was thermally deposited (at a rate of 0.1 nm·s$^{-1}$) onto a chromium adhesion layer (5 nm thick), at a base pressure of approximately $1 \times 10^{-6}$ mbar. The gold-coated samples were cleaned immediately prior to use by placing them in freshly prepared piranha solution for 2 min, followed by a rinse with Milli-Q water.

**SAM Adsorption.** SAMs were formed by immersing the gold-coated slides in 1 mM solutions of the corresponding material, in DCM, over night, at room temperature. The samples were then removed from solution, rinsed with DCM, dried with a nitrogen stream, rinsed with Milli-Q water, and again dried.

**UV Irradiation.** Soft UV (365 nm) light obtained from fluorescent microscope with a power (at the sample) of 40 mW·cm$^{-2}$ was used to irradiate samples mainly for the photo-patterning process. A 365 nm UV lamp (Blak-Ray Model B100 AP) with a nominal power (at the sample) of $4.1 \pm 0.1$ mW·cm$^{-2}$

for 1.5 h ($22 \pm 0.1$ J·cm$^{-2}$ UV dose) was used for wetting, ellipsometry, XPS and FTIR-RAS studies to provide a larger spot size. After the UV irradiation, samples were rinsed with Milli-Q water, isopropanol, dried with a nitrogen stream, rinsed with DCM, and again dried

**Wetting Measurements.** Contact angles were measured using a First-Ten-Angstrom 4000 goniometer under ambient conditions. Milli-Q water droplets were advanced and receded across the surface from a microsyringe needle. Images of advancing and receding droplets were analyzed on both sides of each droplet and typically three values per surface were acquired.

**X-ray Photoelectron Spectroscopy.** Some of the XPS spectra were obtained using a Thermo Scientific ESCA Lab 250 with a chamber pressure maintained below $1 \times 10^{-9}$ mbar during acquisition. A monochromated Al K$_\alpha$ X-ray source (15 kV 150 W) irradiated the samples, with a spot diameter of approximately 0.5 mm. The spectrometer was operated in Large Area XL magnetic lens mode using pass energies of 150 and 20 eV for survey and detailed scans, respectively. Some of XPS spectra were also obtained using a Thermo Scientific K-Alpha XPS system at the National ERSRC XPS Users' Service (NEXUS) at Newcastle University. Samples were irradiated with a monochromated Al K$_\alpha$ Al K$_\alpha$ X-ray source (12 kV 36 W) with a spot diameter of 0.4 mm. The spectrometer was operated with the standard lens using pass energies of 200 and 40 eV for survey and detailed scans, respectively. All of the spectra were obtained with an electron takeoff angle of 90°. High resolution spectra were fitted using CasaXPS (version 2.3.16) peak fitting algorithms. All spectra have been corrected by using C 1s peak at 284.5 eV for charge shifting.

**Fourier Transform-Infrared Reflection Absorption Spectroscopy.** FTIR-RAS spectra were obtained using a Bruker IFS-66 spectrometer equipped with a liquid-N$_2$ cooled MCT detector. The optical path was evacuated. A p-polarized beam at an incident angle of 80° to the surface normal was used for the FTIR measurements. The spectra were taken at a 2 cm$^{-1}$ resolution, and 1000 interferograms were co-added to yield spectra of high signal-to-noise ratio. The reference spectrum was taken from a freshly cleaned gold surface.

**Ellipsometry.** A Jobin-Yvon UVISEL spectroscopic ellipsometer was used to measure the thickness of the SAMs. The wavelength was varied between 400 and 800 nm, in steps of 5 nm. DeltaPsi2 software was used to model and fit the acquired data assuming a simple three-layer system. Values for the base layer (gold support) were obtained from a freshly cleaned gold substrate. The SAM was modeled as a transparent thin film using the Cauchy approximation, $n(\lambda) = A + B.10^4/\lambda^2 + C.10^9/\lambda^4$ and $k(\lambda) = 0$. Where $\lambda$ is the wavelength in units of nanometers and A, B, and C are the Cauchy parameters dependent on optical properties of the material. Parameter, A, was restricted to a value of $1.450 \pm 0.001$ and parameters B and C were allowed to vary. The ambient air was assumed to have $n = 1$ and $k = 0$. Typically, three ellipsometric measurements were made per sample (and on more than one sample of each type).

**Electrochemical cell for electrochemical deposition**. Electrochemical deposition (ECD) was performed by using the SAM modified gold electrode as a working electrode and a Ag/AgCl reference electrode. A coil of platinum wire formed the counter electrode. All electrodes were placed in an electrolyte solution, which was prepared by mixing 10 mM $CuSO_4$ with 10 mM $H_2SO_4$ in an aqueous solution. The ECD was performed using an Autolab PG30 potentiostat. The cyclic voltammograms (CVs) were recorded in the range between -0.30 V and +0.40 V at a scan rate of 10 mV·s$^{-1}$. The appropriate deposition potential was determined from the CV.

**RESULTS AND DISCUSSION**

**Synthesis.** Although lipoic acid derivatives have been promoted as forming particularly good thiol-on-gold SAMs,[23] there are a number of problems associated with their use. The biggest problem is the ease with which lipoic acid and many of its esters undergo polymerization forming linear polydisulfides (Scheme 2). It is known that this polymerization can be induced thermally,[24] chemically,[25,26] photochemically[27,28] or electrochemically.[29]
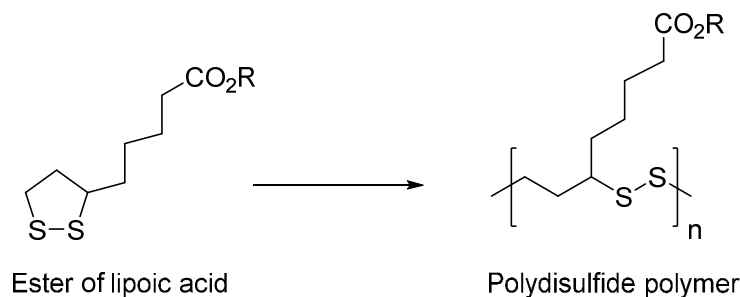
Scheme 2. Polymerization of esters of lipoic acid

Although it was found that the lipoic acid ester **2** was stable in the solid state, at $0^{\circ}$C, for several months

and although dilute solutions were stable for several days at room temperature (as assessed by NMR

spectroscopy or thin layer chromatography), the ester was found to polymerize when attempts were

made to purify it using column chromatography. Recoveries of the ester **2** from conventional column

chromatography on silca (even high grade silica) were very poor. The key to the synthesis (Scheme 1)

was found to be to use the lipoic acid **1** in excess over the acyl bromide so that no unchanged acyl

bromide remained at the end of the reaction. The excess lipoic acid could then be removed by very rapid

passage of a dichloromethane solution through a short 'plug' of silica. However, if stoichiometric

quantities of lipoic acid were used and the reaction failed to go to completion, separation of the

unreacted acyl bromide from **2** required conventional column chromatography which resulted in

polymerization and most of the product was lost.

**SAM Formation.** Characterization of the SAMs produced from lipoic acid **1** and from the ester **2**

suggest that polymerization is not only a problem in the synthesis and chromatography but that it is also

an issue in SAM formation. Most of the early papers on lipoic acid based SAMs show simple

schematics like that in Figure 1(a) which imply that the –S-S- bonds have all been cleaved and that each

ligand molecule is bound to the gold through two Au-S bonds. Naively, this suggests that, compared to a

conventional thiolate SAM [Figure 1(b)], the ligand should be more strongly bound. However, this is

not born out experimentally where force microscopy experiments show that the binding of lipoic acid

derivatives to gold is substantially *weaker* than that of simple thiolates.[30] Furthermore Fig 1(a) cannot be

reconciled with the results of XPS studies of lipoic acid based SAMs which almost always show both 'bound' (Au-S) and 'unbound' (S-H or S-S) sulfur.[31,32] The source and nature of the 'unbound' sulfur revealed by these XPS studies remains unclear. It has been suggested that, for lipoic acid itself, it relates to an ionically bound or hydrogen bonded ad-layer on top of the lipoic acid SAM.[26] However, since we find 'unbound' sulfur for both lipoic acid SAMs and for SAMs of the lipoic acid ester **2** and that this 'unbound' sulfur is not removed by rinsing (Milli-Q water, DCM, isopropanol, methanol or acetonitrile), this explanation seems unlikely. It is more likely that it arises from polysulfide formation.[27] Binding of polysulfide to gold [Figure 1(c)], could give both 'bound' and 'unbound' S signals in the XPS, the proportion of 'unbound' sulfur increasing with the degree of oligomerization. Since dilute solutions were stable for several days at room temperature (as assessed by NMR spectroscopy or thin layer chromatography) may be that this polymerization is promoted by the metal surface.[29] (Reductive opening of the ring followed by chain growth similar to that reported in reference 26)
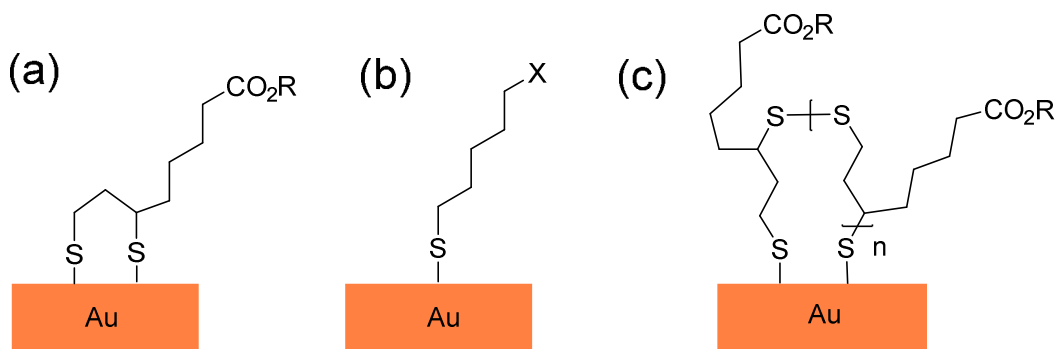
**Figure 1.** Schematic representations of the binding of (a) lipoic acid/lipoic acid derivatives to gold (b) simple thiolates to gold and (c) One way in which oligomers of lipoic acid/lipoic acid esters can bind to gold.

XPS data for the C 1s and O 1s regions for the SAM derived from the ester **2** is shown in Figure 2 and equivalent data for the lipoic acid SAM is shown in the Supporting Information (Figure S4). The XPS for the C 1s region of **2** shows a band at 288.6 eV associated with the C=O carbon[35,36], a band at 287.2 eV attributed to the C-O carbon, a band at 286.3 eV attributed to the C-S carbon and a peak at 284.5 eV assigned to the aliphatic and aromatic carbons and the O 1s region shows peaks for both C=O and C-O.[37-39] The sulfur 2p spectrum is more noisy but, as in related papers, it is best analyzed in terms of two overlapping S 2p spin-orbit doublets created from the two distinct sulfur species; 'bound' and 'unbound' sulfurs. The 'gold-bound' sulfur gives peaks at 161.8 eV and 163.0 eV, which are attributed to the spin-orbit doublet of S $2p_{3/2}$ and S $2p_{1/2}$,.[40,41] The 'unbound' sulfur gives the peaks at 163.3 eV and 164.5 eV, which are also assigned to S $2p_{3/2}$ and S $2p_{1/2}$.[41,42] There is no evidence for oxidized sulfur (usually associated with a peak at 168 eV).[43] Except in terms of peak ratios, the XPS spectrum for the SAM obtained from lipoic acid (supplementary information) is very similar and it also shows both 'bound' and 'unbound' sulfur. The atomic ratios derived from the peak-fittings shown are given in Table 1. These were mainly as expected except that (consistently over a number of samples) the values for the integration in both the carbon and oxygen regions for the ester **2** were high in C-O and low in C=O.

Since all of the analytical and spectroscopic data for compound **2** were correct and since the IR

spectrum for **2** in both KBr and SAM environments (Figure 3) showed both ester and ketone carbonyls

this is not easy to understand. One possibility is that, rather in the same way as aryl nitro groups are

reduced to aryl amino groups under XPS conditions, so possibly there is some reduction of the aryl C=O

to CHOH under these conditions. To test this possibility, the effect of the pyrene residue on the carbonyl

reduction potential was assessed using cyclic voltammetry. This showed that, under these conditions the

first reduction potential of nitrobenzene was -1.386 V versus $Ag/AgNO_3$ that of compound **2** was -1.641

V; that is the aryl keto group is ~255 mV more difficult to reduce than the aryl nitro group (Supporting

Information Figure S5). However, it is easier to reduce than a simple aliphatic ketone which gives some

weight to the suggestion that there may be some reduction of the α-carbonyl group of **2** under XPS

experimental conditions.
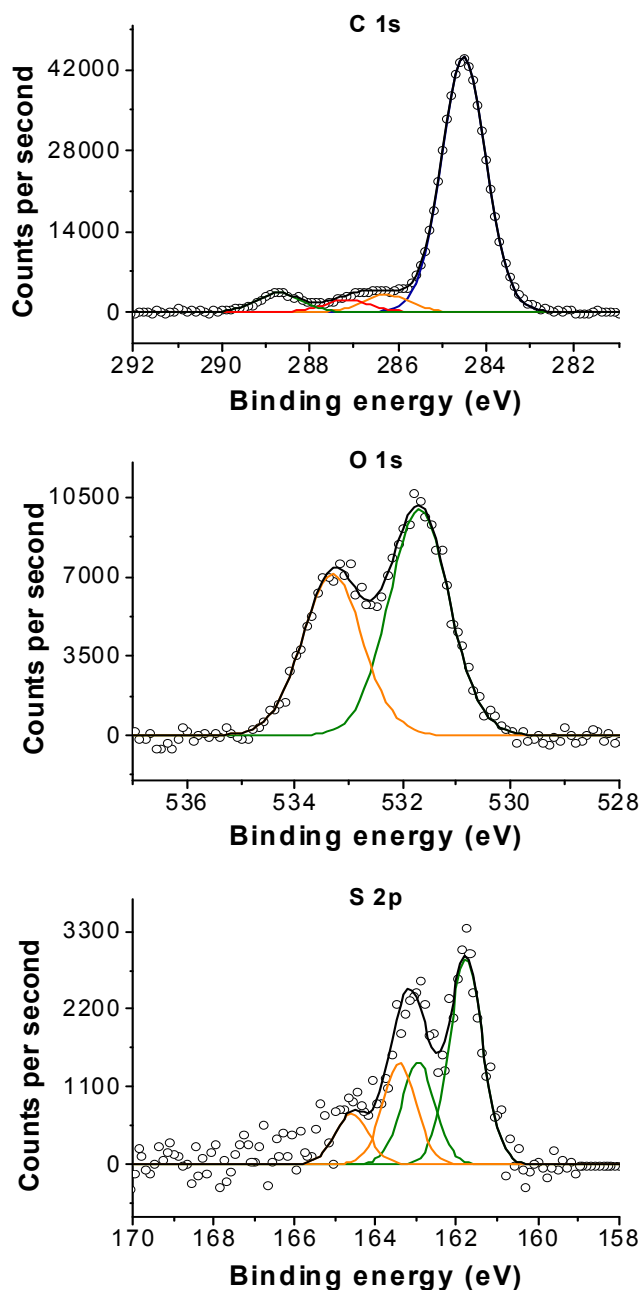
**Figure 2.** XPS data for the SAM derived from the ester **2.** Acquired signal is plotted in open circles and the envelope of the fitted component is represented by the black solid line. (i) (top) C 1s region with four fitted components at gradually increasing binding energy: alkyl/aryl (in blue), C-S (in orange), C-O (in red) and C=O (in green) carbon; (ii) (middle) O 1s region fitted with components corresponding to oxygen in C=O (in green) and C-O group (in orange), respectively; (iii) (bottom) S 2p region fitted with two spin-orbit doublets assigned to thiols bound to gold (in green) and disulfide or unbound thiols (in orange).

**Table 1.** Ratios of integrated (and normalized using relative sensitivity factors) XPS peak areas for

SAMs derived from α-lipoic acid and from the ester **2** normalized to sulfur.

| SAM | Carbon | | | Oxygen | | | Sulfur |
|---|---|---|---|---|---|---|---|
| | C̲=O | C̲-O | Total C | C=O̲ | C-O̲ | Total O | Total S |
| **Lipoic Acid** 1 | 1.3 | - | 9.3 | 1.2 | 1.0 | 2.1 | 2.0 |
| **Expected** 1 | 1.0 | - | 8.0 | 1.0 | 1.0 | 2.0 | 2.0 |
| **Ester** 2 | 1.8 | 1.2 | 29.9 | 1.8 | 1.3 | 3.2 | 2.0 |
| **Expected** 2 | 2.0 | 1.0 | 26.0 | 2.0 | 1.0 | 3.0 | 2.0 |

Table 2 gives the results of water contact angle and ellipsomeric studies of SAMs derived from α-lipoic acid and the ester **2.** The advancing water contact angle for a fresh SAM produced from the ester **2** is $88 \pm 2°$. This is in agreement with that observed for a pyrene terminated SAM on a silicon wafer ($85 \pm 1°$).[44] The thickness of this SAM ($16 \pm 1$ Å) obtained from ellipsometry corresponds to the expected thickness calculated using the length for the fully extended molecule and assuming an average tilt angle relative to the normal of 30°.

**Table 2.** Surface properties of the SAMs derived from lipoic acid **1** and from the ester **2** before and after soft UV (365 nm) irradiation for 1.5 h under a layer of 0.1 M HCl/IPA

| SAMs | Water contact angles (degrees) | | Ellipsometric thickness (Å) | Expected thickness[b] (Å) |
|---|---|---|---|---|
| | $\theta_{Advancing}$ | $\theta_{Receding}$ | | |
| **Lipoic acid** 1 | $30 \pm 2$ | $7 \pm 2$ | $9 \pm 2$ | 8 (9) |
| **Lipoic acid** 1 **after UV**[a] **irradiation under acid for 1.5 h** | $70 \pm 2$ | $18 \pm 4$ | $3 \pm 1$ | 8 (9) |
| **Ester** 2 | $88 \pm 2$ | $62 \pm 6$ | $16 \pm 1$ | 16 (18) |
| **Ester** 2 **after UV**[a] **irradiation under acid isopropanol for 1.5 h** | $89 \pm 2$ | $44 \pm 7$ | $4 \pm 2$ | 8 (9) |
| **Ester** 2 **under acid isopropanol for 1.5 h (no UV)** | | | $17 \pm 1$ | 16 (18) |
| **Ester** 2 **after UV**[a] **irradiation under isopropanol for 1.5 h (no acid)** | $87 \pm 2$ | $51 \pm 3$ | $16 \pm 1$ | 16 (18) |

[a.] Irradiation wavelength = 365 nm, dosage = 22 J·cm$^{-2}$;

[b.] Expected thickness of the SAM using the length of a single molecule estimated from molecular modeling [HyperChem program, semi-empirical (AM1); values given in brackets] assuming a tilt angle of 30° with respect to the surface normal.

Figure 3 shows the FTIR-RAS spectra for the SAMs derived from lipoic acid and the ester **2** compared to the FTIR spectra for these same compounds dispersed in KBr. As expected, and because of the different selection rules which apply to the FTIR-RAS, the relative peak intensities are a little different, but generally there is good agreement. Both the ester **2** SAM and the lipoic acid SAM show peaks corresponding to $CH_2$ stretching in the FTIR-RAS spectrum at 2930 and 2859 cm$^{-1}$ indicating disorder of the alkyl chains (compare to 2919 and 2850 cm$^{-1}$ which we obtain for the SAM layer derived from $C_{18}H_{37}SH$; values typical of ordered SAMs). For the ester **2** the peaks observed between 1600 cm$^{-1}$ and

1450 cm$^{-1}$ are attributed to C=C vibration modes of the pyrene group.[45] The peaks below 1450 cm$^{-1}$

correspond to C-C deformation (~1230-950 cm$^{-1}$), C-H stretching (1217 cm$^{-1}$) and C-H bending in

pyrene rings (819 cm$^{-1}$).[46,47] In the case of lipoic acid there is a marked shift in the acid carbonyl

frequency from that characteristic of the strongly hydrogen bonded dimer in KBr (1693 cm$^{-1}$) to a value

of 1715 cm$^{-1}$ in the SAM layer, which shows that in the SAM there is a reduction in hydrogen bonding.

The ester **2** in KBr shows carbonyl peaks at 1686 (ketone) and 1739 cm$^{-1}$ (ester). In the SAM

environment that for the ketone is slightly shifted to 1694 cm$^{-1}$ whereas that for the ester is essentially

unchanged. Hence the XPS, FTIR-RAS, wetting and ellipsomeric studies are in accord with formation

of the expected SAM structure except that there is apparently some polymerization (some polydisulfide

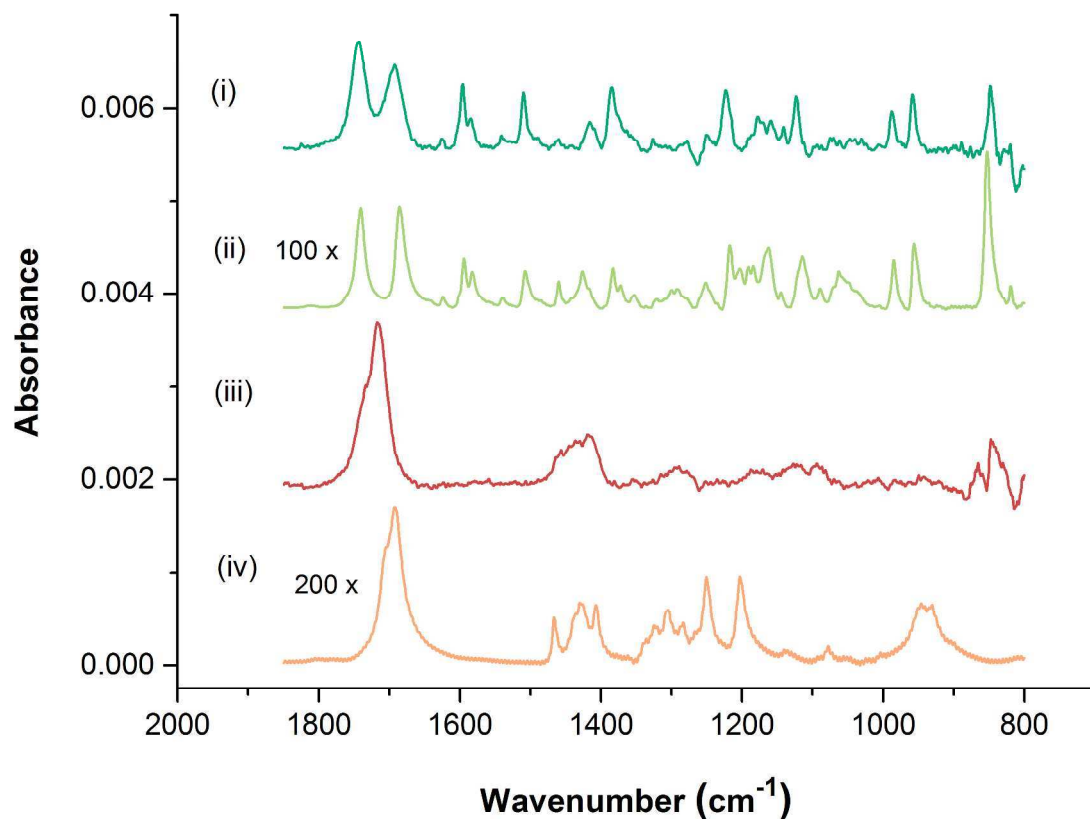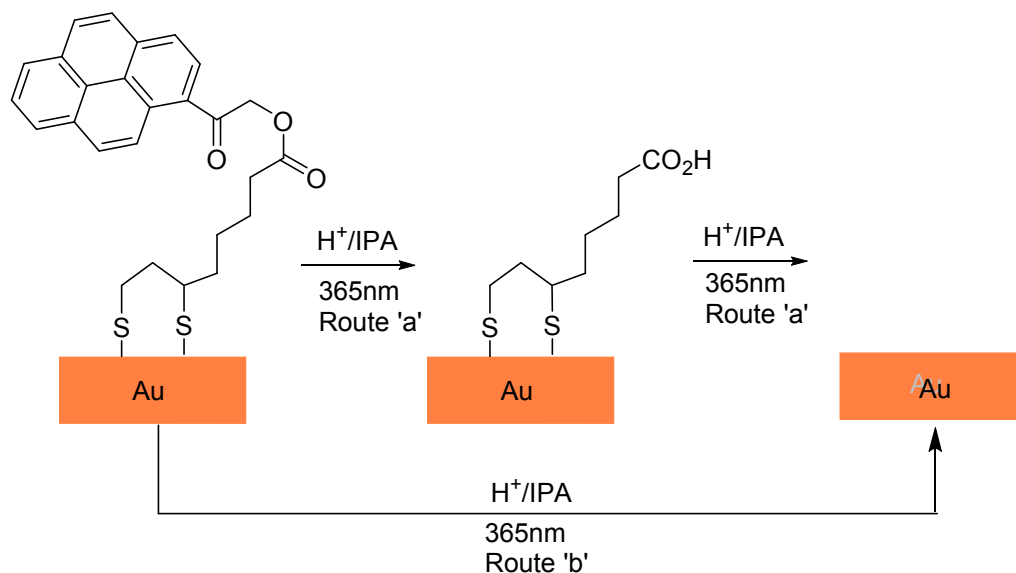formation) for both the lipoic acid and the ester.

**Figure 3.** 800-1850 cm$^{-1}$ regions of the IR spectra. From the top:- (i) (top) FTIR-RAS of the SAM formed from the ester **2** (ii) FTIR of ester **2** dispersed in KBr (iii) FTIR-RAS of the SAM formed form lipoic acid (iv) (bottom) FTIR of lipoc acid dispersed in KBr.

**Scheme 3.** Expected photochemical reaction (photoremoval of the acetylpyrene moiety leading to a

lipoic acid SAM) and two possible explanations of the observed overall process in which the SAM layer

is removed (For simplicity only the form of **2** and of lipoic acid 'bound through both sulfurs' is shown,

see text).

**Soft UV Photolysis of the SAM layers**. Based on literature precedents, we expected that photolysis of

the SAM formed from the ester **2** would result in heterolysis of the α-carbon-to-ester oxygen bond

leading to a gold surface coated with a lipoic acid SAM (Scheme 3).[20,21]  However, whilst the acid

derivative **2** could be photodeprotected in solution, the reaction in the SAM environment was very slow.

This is unlikely to be the result of the red-shift seen in the SAM environment since, although this is of

the order of 25 nm it only shifts the main adsorption maximum to just above rather than just below

365nm and the peaks are very broad. In DCM solution ester **2** shows $\lambda_{max}$ 272, 352 and 384(s) nm

whereas a reflectance UV spectrum of the SAM layer shows $\lambda_{max}$ 296, 376 and 406(s) (Supporting

Information Figure S6). It is much more likely to be a result of the way that gold efficiently quenches

excited states. In general, for soft UV photochemical reactions, quantum yields for organic moieties in

thiol-on-gold SAM layers are generally very much lower than they are in solution.[35]  Based on a report

by Jana *et al.*[20] that, in solution, a higher photoreaction yield for this type of reaction can be achieved by

using a polar solvent (by using a medium that stabilizes the putative ion-pair intermediate shown in

Scheme 3) we then tried photolysis of the SAM under a layer of isopropanol (IPA). When this also

failed to produce a sufficiently rapid photoreaction we tried acid catalysis: photolysis of the SAM under

a layer of 0.1 M HCl in IPA (we tried using a proton to capture the anion within the ion pair). This

proved to be much more successful.  FTIR-RAS data for this photoreaction is shown in Figure 4, the

XPS data in Figure 5 and the wetting and ellipsometry results in Table 2. The top of Figure 4 shows the

FTIR-RAS spectrum of the SAM derived from the ester **2**. As can be seen from the two spectra

immediately below it, there is no change when this SAM is photolyzed through a layer of IPA or when

it is left in contact with 100 mM HCl in IPA 'in the dark'. However, a substantial difference is

noticeable when the SAM is photolyzed through a 100 mM solution of HCl in IPA, although the

spectrum obtained does not correspond with that for the expected product: a SAM composed of lipoic

acid (bottom trace). What rather seems to have happened is that the amount of compound **2** on the

surface is reduced. This is confirmed by the XPS results. When the SAM is photolyzed through a 100

mM solution of HCl in IPA the total amount of carbon, oxygen and sulfur decrease but the relative

amounts of these three components before and after photolysis is almost the same (Supporting

Information, Figure S7). The only clear difference in the peak shapes (or indeed the ratios of the

elements) is a change in the shape of the S 2p region which corresponds to there being relatively less

'unbound sulfur', relatively more 'bound' sulfur after photolysis. It appears that there is acid-catalyzed

photo-removal of the lipoic acid layer as it is formed. That lipoic acid is indeed removed from the

surface under these conditions is shown by the XPS.  Starting from a SAM prepared from α-lipoic acid

and photolyzing under identical conditions it is seen that the carbon, oxygen and sulfur signal all

diminish and, once again, the only noticeable difference in the relative peak intensities is that after

photolysis there is relatively less 'unbound sulfur', relatively more 'bound' sulfur.
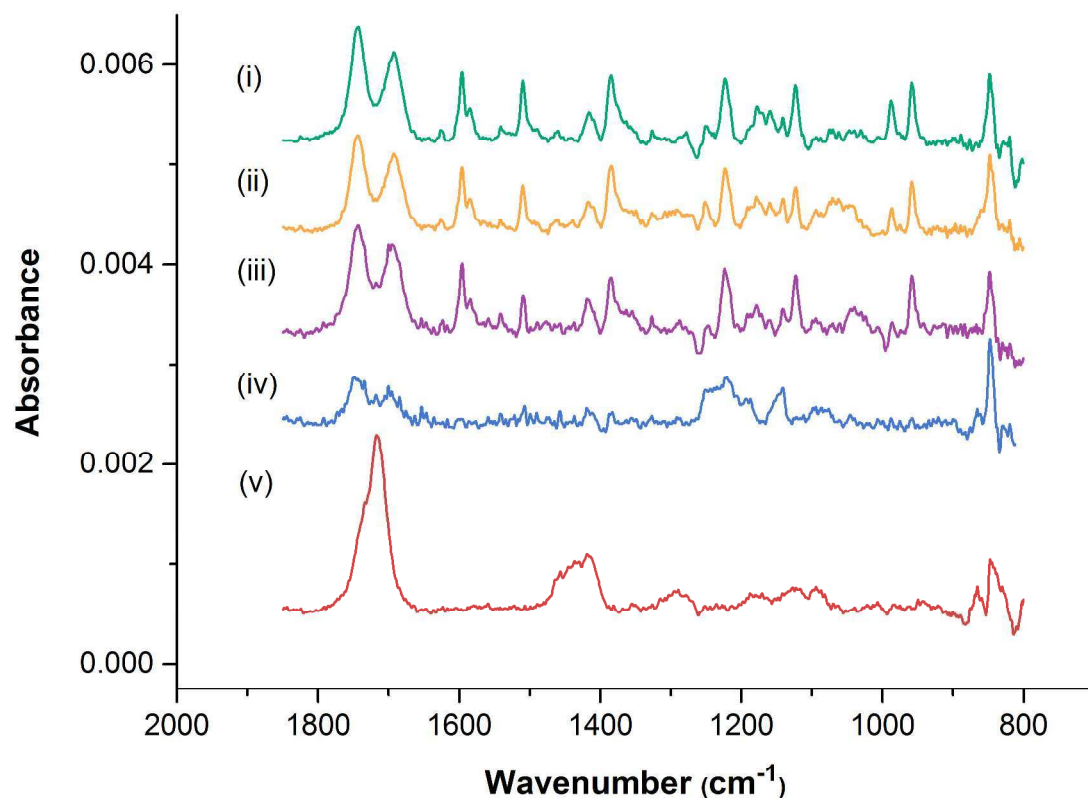
**Figure 4.** 800-1850 cm$^{-1}$ regions of the FTIR-RAS spectra. From the top:- (i) (top) FTIR-RAS of the SAM formed from the ester **2** (ii) FTIR-RAS of the SAM formed from the ester **2** after 1.5 h photolysis under a layer of IPA (iii) FTIR-RAS of the SAM formed from the ester **2** after 1.5 h storage (without UV) under a layer of 100 mM HCl in IPA (iv) FTIR-RAS of the SAM formed from the ester **2** after 1.5 h photolysis under a layer of 100mM HCl in IPA (v) (bottom) FTIR-RAS of the SAM formed form lipoic acid.

.**Electrodeposition of copper on patterned photolyzed SAM layers.** When the SAM derived from

ester **2** was photolyzed through a mask (15 min of UV exposure time under the microscope producing

40 mW·cm$^{-2}$ power at the sample) patterned substrates were produced and then these were used for the

regioselective electrochemical deposition (ECD) of copper from an acidic copper sulfate solution. At a

controlled potential it is easy to selectively grow a layer of copper on the photolyzed regions and this

layer can be cleanly removed by reversing the electrode potential. This process is wholly reversible over

at least ten cycles.



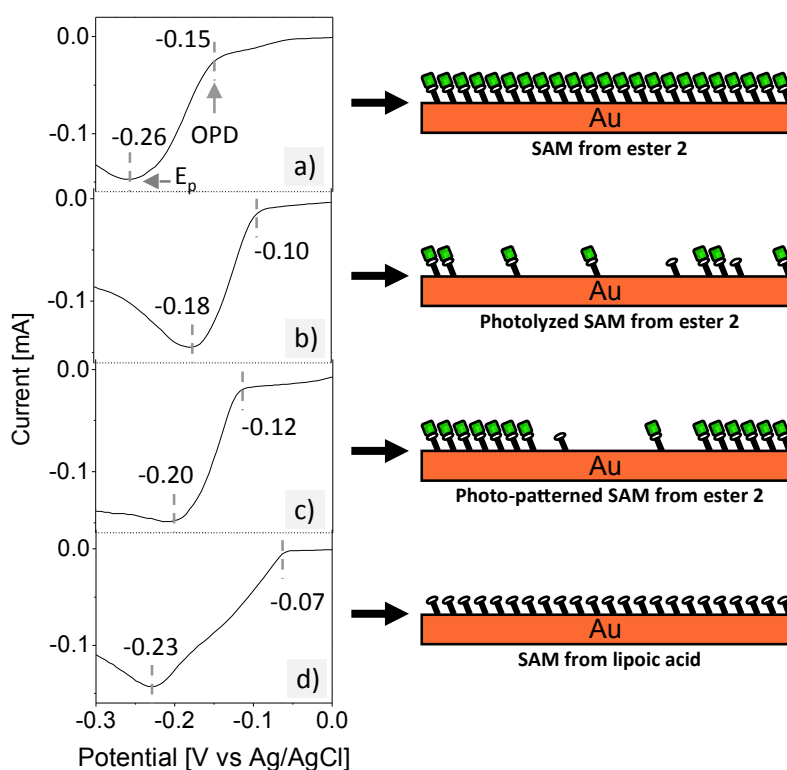**Figure 5.** (left) Cyclic voltammograms corresponding to the reduction of a solution of 10 mM CuSO$_4$ in

10 mM H$_2$SO$_4$. (right) schematic representations of the SAM layers. a) SAM derived from the ester **2**, b)

SAM derived from the ester **2** after photolysis. c) photo-patterned SAM (200 μm × 150 μm stripes) d)

lipoid acid SAM. The tenth cycle for each sample is presented. Scan rate 10 mV·s$^{-1}$.

Figure 5 shows cyclic voltammograms (CVs) for the reduction of an acidic copper sulfate solution on

various SAM-modified gold electrodes (10 mM $CuSO_4$ in 10 mM $H_2SO_4$ solution; scan rate 10 mV·$s^{-1}$).

The equilibrium potential, also known as an open cell potential (OCP), was observed to be +0.03 V in

all cases and it was not significantly different from that of bare gold. The overpotential required for

deposition of copper (the OPD) for a SAM-modified cathode is mainly determined by the thickness of

the SAM. Hence the OPD values observed more-or-less follow the expected order: SAM from ester **2** (-

0.15 V) > photo-patterned SAM from ester **2** (-0.12 V) > photocleaved SAM from ester **2** (-0.10 V) >

lipoic acid SAM (-0.07 V). The monolayer thicknesses measured by elipsometry being: SAM from ester

**2** (16 ± 1 Å) > photo-patterned SAM from ester **2** > lipoic acid SAM (9 ± 2 Å) > photocleaved SAM

from ester **2** (4 ± 2 Å). At potentials more negative than the OPD, the reduction rate for $Cu^{2+}$ depends on

the electron transfer and the $Cu^{2+}$ diffusion rates, which cause a dramatic increase in the current value.

The maximum current value, where the reduction rate is limited by the diffusion of $Cu^{2+}$ ions to the

cathode, is called limiting diffusion current ($I_p$). The potential at which this limiting current is reached is

known as the peak potential ($E_p$). Figure 5 shows the $E_p$ values for the different SAMs. These are in the

order ester SAM from ester **2** > lipoic acid SAM (-0.23 V) > photo-patterned SAM from ester **2** (-0.20

V) > photocleaved SAM from ester **2** (-0.18 V). On patterned surfaces, the significant difference of $E_p$

for the photolyzed (-0.18 V) and unphotolyzed (-0.26 V) ester SAMs could be utilized for spatially

selective electrochemical deposition of copper. Figure 6 shows a cyclic voltammogram for a patterned

SAM (CVs) between -0.30 V and +0.40 V (scan rate of 10 mV·$s^{-1}$) together with optical images taken at

different potentials showing the deposition and removal of the copper on the stripes which had been

exposed to the UV light. The CV started at 0 V (position **1**), where no nucleation of copper was

observed on surface. At -0.18 V (position **2**), the limiting diffusion current ($I_p$) for the photocleaved

SAM deposition of Cu leads to an appearance of bright regions (200 μm wide) covered by a high

density of copper particles. Even at -0.26 V (position **3**) there is very little deposition of copper on the

unphotolyzed stripes. The 1-acetylpyrene functionalized SAM acts as a very efficient barrier to copper

deposition. At more positive potential than the OCP (position **4**) $Cu^0$ is oxidized back to $Cu^{2+}$ but a low

density of copper particles is still observed. Finally, the copper was completely removed from SAMs surface at +0.20 V (position **5**). Hence, the deposition/stripping of copper on the photo-patterned SAM is highly selective and reversible. The process could be repeated for over at least ten cycles.
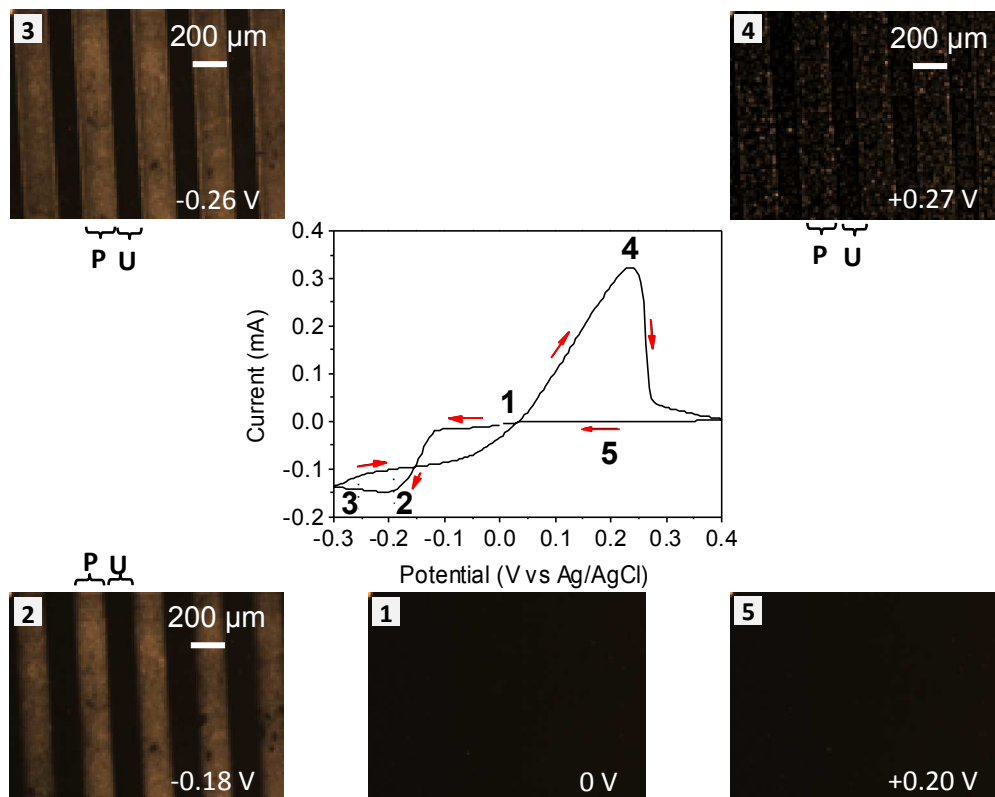


**Figure 6.** Cyclic voltammograms (CVs) for the electrodeposition of copper on the photo-patterned SAM at a scan rate of 10 mV·s$^{-1}$. The traces for four of the ten cycles (numbers 5,7,9,10) have been overlaid (there is virtually no difference between them). The images which show the growth of the copper on the photolyzed stripes were taken from a video which was captured at the same time as the CV data. Photolyzed (**P**) and unphotolyzed (**U**) regions are on 200 μm and 150 μm wide respectively.

**The generality of the acid-catalyzed removal of thiol-on-gold SAMs using soft UV light.** The most surprising, unexpected feature of this study is the finding that the SAM formed from lipoic acid and from the ester **2** can be removed (or at least partially removed) from gold using a combination of soft UV light and acid catalysis. Surprising, because this sort of process was not reported in any of the

previous studies in which thiol-on-gold SAMs were photolyzed through an acidified alcohol layer and because there is no obvious molecular 'chromophore' in lipoic acid that absorbs significantly at 365 nm. Possibly absorption in this region arises from sulfur-sulfur interactions within the SAM or from the Au-S 'bond' or is related to protonation of sulfur. To try to understand whether this is a general phenomenon or whether it is something specific to the (rather weakly bound) lipoic acid SAM we decided to study the behavior of a number of SAMs under these reaction conditions. Namely the SAMs obtained from dithiobutyric acid DTBA [$AuS(CH_2)_3CO_2H$], from mercaptohexanoic acid MHA [$AuS(CH_2)_5CO_2H$], from mercaptooctanoic acid MOA [$AuS(CH_2)_7CO_2H$] and from mercaptoundecanoic acid MUA[$AuS(CH_2)_{10}CO_2H$]. What transpired was that, under soft UV irradiation and acid catalysis, cleavage from the surface is a general phenomenon; at least for the shorter, more disordered SAM layers. Table S1 (Supporting Information) shows the ellipsometric and wetting angle data for all of these SAM layers under identical reaction conditions. The ellipsometry data shows that there is marked decrease in thickness for the DTBA, MHA, and lipoic acid SAMs and that for MOA and MUA the thickness is (within experimental error) unchanged. The FTIR-RAS studies (Supporting Information, Figure S8) show loss of most of the carbonyl adsorption for DTBA and MHA but very little change for MOA. The XPS studies (Supporting Information, Figure S9) show a roughly 60% reduction in the signal intensity for DTBA and MHA, a roughly 20% reduction for MOA but little or no change in the signal intensities for MUA. In Figure 7 the XPS data for all six SAMs is displayed graphically; the fractional decrease in the intensity of the XPS peaks for carbon (carbonyl carbon), oxygen and sulfur being plotted against the initial thickness of the SAM layer. Note that the fractional decrease for all three elements (carbon, oxygen and sulfur) is about the same. The ratio also remains the same but the amount of material on the surface decreases. Note also that the fractional decrease depends on the initial thickness of the SAM layer with the MUA layer being virtually unaffected. Both acid catalysis and 365nm UV are required. There is no effect when these SAMs are irradiated in the IPA on its own (in the absence of acid) or when they are kept under acidic IPA in absence of UV light. Taken together, these results show that the photocleavage process is dependent on the thickness and/or possibly the ordering

within the SAM.  It is clear that this is a very different process to the general degradation of SAM layers

that occurs under hard UV irradiation (because of the chain length/SAM layer thickness dependence). It

is also important to note that the process is not one of thermal desorption of the SAM from the surface

of the gold. This idea would be difficult to reconcile with the chain-length dependence of the fractional

change in thickness shown in Figure 7. Furthermore, it would be inconsistent with the IR and

ellipsometric data (Figure 4 and Table 1) shown for ester **2** and for lipoic acid when photolysed under

isopropanol with and without added acid or when kept for 1.5 h without UV exposure under acidic

isopropanol.
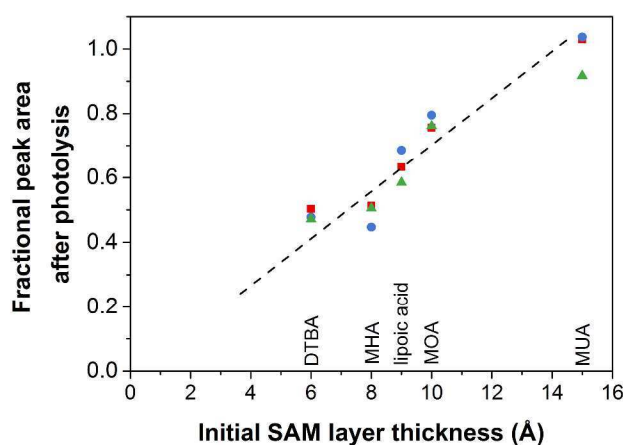


**Figure 7**. Fractional changes for the five acid-terminated SAMs in the area of the peaks (normalized

relative to gold) for carbonyl carbon (squares), oxygen (circles) and sulfur (triangle) plotted against the

measured initial thickness of the SAM layer. The straight line is intended only as a guide to the eye.

Photolysis conditions: 365 nm; 1.5 h; under a layer of 0.1 M HCl/IPA; 365 nm dosage = 22 J·cm$^{-2}$. The

data for carbonyl carbon is chosen since, under prolonged exposure, the 'total carbon' showed evidence

of contamination from atmospheric hydrocarbons.

**CONCLUSION**

A thiol-on-gold SAM based on a 1-acetylpyrene protected carboxylic acid functional group has been

prepared and characterized. Photolysis of this SAM using soft UV (365 nm) under an acidic ad-layer

was found to be more effective than direct photolysis in the air or photolysis under an ad-layer of a polar

solvent but (unexpectedly) it was found that the photolysis product (the lipoic acid) is also removed

from the surface under these conditions. The significant increase in the peak potential ($E_p$); the way in

which the 1-acetylpyrene group of the unphotolysed SAM blocks the electrodeposition of copper means

that these photo-patterned SAMs are very suitable for the spatially selective electrodeposition of copper.

The most unexpected finding to arise from these studies is that the SAMs derived from DTBA, MHA

and lipoic acid are also partially removed from the surface on irradiation with 365 nm light through a

solution of 0.1 M HCl in IPA. This process is chain-length (SAM thickness and/or order) dependent.

The fact that the longer chain SAMs are more stable suggests that the overall process observed in the

photolysis of the pyrene ester **2** is probably one in which photocleavage of the pyrene residue leads to a

lipoic acid residue which is then cleaved from the surface (Route 'a' in Scheme 3) rather than one in

which there is direct removal of the pyrene ester from the surface (Route 'b' in Scheme 3). The fact that

the shorter chain SAMs are partially removed from the surface but those based on longer chains are

more stable may suggest that the proton participates directly in the Au-S bond cleavage process.

Alternatively, this may be related to the fact that these longer chain SAMs are more ordered and perhaps

the thiol, disulfide or protonated disulfide cleaved from the surface is then more likely to recombine

with the gold rather than diffuse away into the solution. Regardless of these speculations it is clear that

acid catalyzed photolyses of thiol-on-gold SAMs, certainly photolyses that require the sort of dosage

used in this study (22 J·cm$^{-2}$),  need to be used with caution.


**ASSOCIATED CONTENT**

**Supporting Information**

NMR data for compound **2**. XPS data for the SAM derived from lipoic acid, Cyclic voltammetry data

for solutions of nitrobenzene and the pyrene ester **2,** UV/vis spectra for the ester **2** in solution and in the

SAM environment, XPS data for SAMs derived from ester **2** and from lipoic acid both before and after

photolysis,  FTIR-RAS spectra for DTBA, MHA and MOA SAMs before and after photolysis,  XPS

data for the acid-catalysed photolysis of SAMs of DTBA, MHA, MOA and MUA. The Supporting

Information is available free of charge on the ACS Publications website at…………

## AUTHOR INFORMATION

### Corresponding Author

Tel.: +44 (0)113 343 6509. Fax: +44 113 343 6565. E-mail: r.j.bushby@leeds.ac.uk

### ORCHID

Richard J. Bushby 0000-0002-1627-6058

### Notes

The authors declare no competing financial interest.

REFERENCES

 (1) Ivashenko, O.; van Herpt, J. T.; Feringa, B. L.; Rudolf, P.; Browne, W. R. UV/Vis and NIR Light-Responsive Spiropyran Self-Assembled Monolayers *Langmuir* **2013**, *29*, 4290-4297.

(2) Prompinit, P.; Achalkumar, A. S.; Walton, A. S.; Bushby, R. J.; Walti, C.; Evans, S.D. Reversible Metallization of Soft UV Patterned Substrates *J. Mater. Chem. C* **2014**, *2*, 5916-5923.

(3) Yang, Y. M.; Shao, Q.;  Deng, R. R.; Wang, C.; Teng, X.; Cheng, K.; Cheng, Z.; Huang, L.; Liu, Z.; Liu, X. G.; Xing, B. G. In Vitro and In Vivo Uncaging and Bioluminescence Imaging by Using Photocaged Upconversion Nanoparticles *Angew. Chem. Int. Ed.* **2012**, *51*, 3125-3129.

(4) Yang, Y. M.; Velmurugan, B.; Liu, X.G.; Xing, B.G. NIR Photoresponsive Crosslinked Upconverting Nanocarriers Toward Selective Intracellular Drug Release *Small* **2013**, *9*, 2937-2944.

(5) Nakagawa, M.; Ichimura, K. Photopatterning of Self-Assembled Monolayers to Generate Aniline Moieties *Colloids Surf. A* **2002**, *204*, 1-7.

(6) Critchley, K.; Jeyadevan, J. P.; Fukushima, H.; Ishida, M.; Shimoda, T.; Bushby, R. J.; Evans, S.D. A Mild Photoactivated Hydrophilic/Hydrophobic Switch *Langmuir* **2005**, *21*, 4554-4561.

(7) Zhao, B.; Moore, J. S.; Beebe, D. J. Principles of Surface-Directed Liquid Flow in Microfluidic Channels *Anal. Chem.* **2002**, *74*, 4259-4268.

(8) Prompinit, P.; Achalkumar, A. S.; Han, X. J.; Bushby, R. J.; Walti, C.; Evans, S. D. Improved Photoreaction Yields for Soft Ultraviolet Photolithography in Organothiol Self-Assembled Monolayers *J. Phys. Chem. C* **2009**, *113*, 21642-21647.

(9) Lo, M. K. F.; Gard, M. N.; Goldsmith, B. R.; Garcia-Garibay, M. A.; Monbouquette, H. G. Synthesis and Micropatterning of Photocatalytically Reactive Self-Assembled Monolayers Covalently Linked to Si(100) Surfaces via a Si-C Bond *Langmuir* **2012**, *28*, 16156-16166.

(10) El Zubir, O.; Barlow, I.; Ul-Haq, E.; Tajuddin, H. A.; Williams, N. H.; Leggett, G. J. Generic Methods for Micrometer- And Nanometer-Scale Surface Derivitization Based on Photochemical Coupling of Primary Amines to Monolayers of Aryl Azides on Gold and Aluminum Oxide Surfaces *Langmuir* **2013**, 29, 1083-1092.

(11) Martin, T. A.; Herman, C. T.; Limpoco, F. T.; Michael, M. C.; Potts, G. K.; Bailey, R. C. Quantitative Photochemical Immobilization of Biomolecules on Planar and Corrugated Substrates: A Versatile Strategy for Creating Functional Biointerfaces *ACS Appl. Mater. Interfaces* **2011**, *3*, 3762-3771.

(12) Kim, S.-H.; Ohtsuka, H.; Tria, M. C. R.; Tanaka, K.; Advincula, R. C.; Usui, H. Preparation of Surface-Tethered Polymer Layer on Inorganic Substrates by Photoreactive Self-Assembled Monolayer *Thin Solid Films* **2014**, 554, 78-83.

(13) Nakano, K.; Matsunaga, H.; Sai, K.; Soh, N.; Imato, T. Photoactive Covalent Attachment of Deoxyribonucleic Acid on Gold with Double-Strand Specificity using Self-Assemble Monolayers Containing Psoralen *Anal. Chim. Acta* **2006**, *578*, 93-99.

(14) Tsuchiya, Y.; Haraguchi, S.; Ogawa, M.;. Shiraki, T.; Kakimoto, H.; Gotou, O.; Yamada, T.; Okumoto, K.; Nakatani, S.; Sakanoue, K.; Shinkai, S. Fine Wettability Control Created by a Photochemical Combination Method for Inkjet Printing on Self-Assembled Monolayers *Adv. Mater.* **2012**, *24*, 968-972.

(15) Yu, Y.; Kang, X.M.; Yang, X.S.; Yuan, L.H.;  Feng, W.; Cui, S.X. Surface Charge Inversion of Self-Assembled Monolayers by Visible Light Irradiation:Cargo Loading and Release by Photoreactions *Chem. Commun.* **2013**, *49*, 3431-3433.

(16) Critchley, K.; Ducker, R.; Bramble, J. P.; Zhang, L.; Bushby, R. J.; Leggett G. J.; Evans, S. D. Photodeprotection Patterning of Self-Assembled Monolayers *J. Exp. Nanosci.* **2007**, *2*, 278-290.

(17) Stegmaier, P.; Alonso, J. M.; del Campo, A. Photoresponsive Surfaces with Two Independent Wavelength-Selective Functional Levels *Langmuir* **2008**, *24*, 11872-11879.

(18) San Miguel, V.; Bochet, C. G.; del Campo, A. Wave-Length-Selective Caged Surfaces: How Many Functional Levels are Possible *J. Amer. Chem. Soc.* **2011**, *133*, 5380-5388.

(19) Alvarez, M.; Best, A.; Ungar, A.; Alonzo, J. M.; del Campo, A.; Schmelzeisen, M.; Koynov, A; Kreiter Near-Field Lithography by Two-Photon Induced Photoclevage of Organic Monolayers *Adv. Mater.* **2010**, *20*, 4265-4272.

(20) Jana, A.; Atta, S.; Sarkar, S. K.; Singh, N. D. P. 1-Acetylpyrene with Dual Functions as an Environment-Sensitive Fluorophore and Fluorescent Photoremovable Protecting Group *Tetrahedron* **2010**, *66*, 9798-9807.

(21) Klan, P.; Solomek, T.; Bochet, C. G.; Blanc, A.; Givens, R.; Rubina, M.; Popik, V.; Kostikov, A.; Wirz, J. Photoremovable Protecting Groups in Chemistry and Biology: Reaction Mechanisms and Efficiency *Chem. Rev.* **2013**, *113*, 119-191.

(22) Zhao, L.; Chen, D.; Hu, W. Patterning of Metal Films on Arbitrary Substrates by Using Polydopamine as a UV-Sensitive Catalytic Layer for Electroless Deposition *Langmuir* **2016**, *32*, 5285-5290.

(23) Daengngam, C.; Thorpe, S. B.; Guo, X.; Stoianov, S. V.; Santos, W. L; Morris, J. R.; Robinson, H. D. High Photoreactivity of o-Nitrobenzyl Ligands on Gold *J. Phys. Chem. C* **2013**, *117*, 14165-14175.

(24) Kisanuki, A.; Kimpara, Y.; Oikado, Y.; Kada, N.; Matsumoto, M.; Endo, K. Ring-Opening Polymerization of Lipoic Acid and Characterization of the Polymer *J. Polym. Sci. Part A: Polym. Chem.* **2010**, *48*, 5247-5253.

(25) Bang, E.-K.; Ward, S.; Gasparini, G.; Sakai, N.; Matile, S. Cell-Penetrating Poly(disulfide)s: Focus on Substrate-Initiated Co-Polymerization *Polym. Chem.* **2014**, *5*, 2433-2441.

(26) Areephong, J.; Ortenas, E.; Saki, N.; Matile, S. Directional Stack Exchange along Oriented Oligothiophene Stacks *Chem. Commun.* **2012**, *48*, 10818-10620.

(27) Barltrop, J. A.; Hayes, P. M.; Calvin, M. The Chemistry of 1,2-Dithiolane (Trimethylene Disulfide) as a Model for the Primary Quantum Conversion Act in Photosynthesis *J. Am. Chem. Soc.* **1954**, *76*, 4348-4367.

(28) Brown, P. R.; Edwards, J. O. Effect of Solvent on the Photolysis of Alpha-Lipoic Acid *J. Org. Chem.* **1969**, *34*, 3131-3135.

(29) Krishnan, C. V.; Garnett, M. Electrochemical Behaviour of the Super Antioxidant, Alpha-Lipoic Acid *Int. J. Electrochem. Sci.*, **2011**, *6*, 3607-3630.

(30) Langry, K. C.; Ratto, T. V.; Rudd, R. E.; McElfresh, M. W. The AFM Measured Force Required to Rupture the Dithiolate Linkage of Thioctic Acid to Gold is Less than the Rupture Force of a Simple Gold-Alkyl Thiolate Bond *Langmuir* **2005**, *21*, 12064-12067.

(31) Willey, T. M.; Vance, A. L.; Bostedt, C.; van Buuren T.; Meulenberg, R. W.; Terminello, L. J.; Fadley, C. S. Surface Structure and Chemical Switching of Thioctic Acid Adsorbed on Au(111) as Observed using Near-Edge X-Ray Adsorption Fine Structure *Langmuir* **2004**, *20*, 4939-4944.

(32) Volkert, A. A.; Subramanian, V.; Ivanov, M. R.; Goodman, A. M.; Haes, A. J. Salt-Mediated Self-Assembly of Thiotic Acid on Gold Nanoparticles *ACS Nano*, **2011**, *5*, 4570-4580.

(33) Volkel, B.; Kaltenpoth, G.; Handrea, M.; Sahre, M.; Nottbohm, C. T.; Kuller, A.; Paul, A.; Kautek, W.; Eck, W.; Golzhauser, A. Electrodeposition of Copper and Cobalt Nanostructures using Self-Assembled Monolayer Templates *Surf. Sci.* **2005**, *597*, 32-41.

(34) Song, J.; Noh, H.; Lee, H.; Lee, J.-N.; Lee, D.J.; Lee, Y.; Kim, C.H.; Lee, Y.M.; Park, J.-K.; Kim, H.-T. Polysulfide Rejection Layer from Alphalipoic Acid for High-Performance Lithium-Sulfur Battery *J. Mater. Chem. A* **2015**, *3*, 323-330.

(35) Critchley, K.; Zhang, L. X.; Fukushima, H.; Ishida, M.; Shimoda, T.; Bushby, R. J.; Evans, S. D. Soft-UV Photolithography using Self-Assembled Monolayers *J. Phys. Chem. B* **2006**, *110*, 17167-17174.

(36) Bain, C. D.; Troughton, E. B.; Tao, Y. T.; Evall, J.; Whitesides, G. M.; Nuzzo, R. G. Formation of Monolayer Films by Spontaneous Assembly of Organic Thiols from Solution onto Gold *J. Am. Chem. Soc.* **1989**, *111*, 321-335.

(37) Beamson, G.; Briggs D. *High Resolution XPS of Organic Polymers The Scienta ESCA300 Database*; Wiley: Chichester, UK, 1992.

(38) Ohnishi, S.; Ishida, T.; Yaminsky, V. V.; Christenson, H. K. Characterization of Fluorocarbon Monolayer Surfaces for Direct Force Measurements *Langmuir* **2000**, *16*, 2722-2730.

(39) Artyushkova, K.; Fulghum, J. E.; Reznikov, Y. Orientation of 5CB Molecules on Aligning Substrates Studied by Angle Resolved X-ray Photoelectron Spectroscopy *Mol. Cryst. Liq. Cryst.* **2005**, *438*, 1769-1777.

(40) Kalimuthu, P.; Kalimuthu, P.; John, S. A. Leaflike Structured Multilayer Assembly of Mercaptothidiazole on Gold Surface *J. Phys. Chem. C* **2009**, *113*, 10176-10184.

(41) Sun, F.; Castner, D. G.; Grainger, D. W. Ultra-thin Self-Assembled Polymer Films on Solid Surfaces 2. Formation of 11-(N-pentyldithio)undecanoate-Bearing Polyacrylate Monolayers on Gold *Langmuir* **1993**, *9*, 3200-3207.

(42) Iida, T.; Sakai, Y.; Shimomura, T.; Nakamura, T.; Ito, K. Chemical Adsorption of Poly(3-alkylthiophene) on Au using Self-Assembly Technique *Jpn. J. Appl. Phys., Part 2* **2007**, *46*, L1126-L1128.

(43) Wang, W. Z.; Huang, P. C. Influences of Branched Side Chains and Cross-Linking Network on the Solid State Structures of Oligo- and Poly(p-phenyleneethynylene)s *J. Macromol. Sci., Part B: Phys.* **2007**, *46*, 1081-1092.

(44) Lu, F.; Fang, Y.; Blanchard, G. J. Probing the Microenvironment of Surface-Attached Pyrene Formed by aThermoresponsive Oligolmer *Spectrochim. Acta, Part A* **2009**, *74*, 991-999.

(45) Nakanishi, K. *Infrared absorption spectroscopy, practical*; Holden Day: San Fransisco, 1962.

(46)Toriumi, H.; Sugisawa, H.; Watanabe, H. Time-Resolved FT-IR Study of Electric-Field Induced Homogeneous-to-Homeotropic Transition of Nematic 4-Pentyl-4'-cyanobiphenyl *Jpn. J. Appl. Phys., Part 2* **1988**, *27*, L935-L937.

(47) Jbarah, A. A.; Doering, K.; Lang, H.; Holze, R. Stectrochemical Studies of Self-Assembled Monolayers of Biphenyl Ethynyl  Thiols on Gold Electrodes *Vib. Spectrosc.* **2009**, *49*, 162-173.

200µm

H⁺/UV
(365 nm)

Cu²⁺/+e⁻

Au

Au

Au

Au